学位論文（要約）

Carrier-envelope-phase dependence of asymmetric C-D bond breaking in C_2D_2 by few-cycle laser pulses

（数サイクルレーザーパルスによる C_2D_2 の非対称 C-D 結合切断 における搬送波位相依存性 ）

平成 25 年 12 月　博士（理学）申請

東京大学大学院理学系研究科
化学専攻
三浦　瞬

Abstract

The present thesis starts with a general introduction of the atomic and molecular dynamics induced by few-cycle intense laser pulses followed by Chapter 2, in which the experimental setup prepared for the investigation of CEP dependences of molecular dynamics is described. Few-cycle pulses were generated from the output of a Ti:Sapphire laser system with a rare-gas filled hollow-core fiber and a set of chirp mirrors. The few-cycle pulses were divided into two beams. One of them was introduced into a phasemeter in which the CEP of the few-cycle pulses can be measured shot-by-shot. The other of the divided beams was focused onto a sample gas in a momentum imaging chamber. The data measured in the two apparatuses were recorded simultaneously, and the CEP dependence of the molecular process was measured.

In the Chapter 3, the carrier envelope phase (CEP) dependence in the C-D bond breaking of C_2D_2 induced by an intense few-cycle laser pulse was investigated. The ejection direction of D^+ ions generated from the Coulomb explosion, $C_2D_2^{2+} \rightarrow C_2D^+$ and D^+, exhibited the CEP dependent asymmetry, while its CEP dependence was out of phase by π with respect to the CEP dependence of the recoil momentum of $C_2D_2^+$. From a recollisional double ionization model, the asymmetry in the ejection direction of D^+ was ascribed to the laser-assisted C-D bond weakening in the few-cycle laser field.

Finally, in Chapter 4, the conclusion of the present thesis and the future perspective are described.

Contents

Chapter 1. General Introduction

1.1 Molecular dynamics induced by intense laser fields

Thanks to the chirped pulse amplification method (CPA) invented in 1985 [1], an intense laser field whose magnitude is larger than 10^{14} W/cm^2 can now routinely be generated by focusing pulses of a CPA laser. When molecules are exposed to such an intense laser field, high order non-linear optical processes such as multi-photon excitation and ionization are induced. Through the investigation of responses of molecules to an intense laser field, we can extract the information of the ultrafast motion of atoms and electrons within a molecule on the femtosecond time scale.

Ultrafast laser pulses are characterized by several parameters such as their intensity, wavelength and pulse duration. During the doctor course period, I investigated the effect of another important parameter called the "carrier-envelope phase (CEP)" on molecular processes induced by ultrashort laser pulses. In Chapter 2, I will describe an experimental setup I developed for investigating CEP dependent molecular processes. The experimental setup consists of the following three parts: (i) the method of few-cycle pulse generation, (ii) a momentum imaging apparatus by which the molecular dynamics is investigated through the detection of the generated ions, and (iii) a phasemeter with which the CEP of respective few-cycle pulses is measured. In Chapter 3, I will describe a CEP dependent asymmetric dissociation process of deutrated acetylene. The origin of the asymmetry is discussed in terms of recollisional double ionization and subsequent electron density variation within a molecular ion induced by the laser fields.

1.2 Intense laser for molecular science

Ultrashort dynamics of molecules induced by an intense laser field has been studied by detecting emitted photoelectrons and/or fragment ions using a time-of-flight (TOF) type mass spectrometer. When intense laser pulses are linearly polarized, the angular distribution of the emission direction of fragment ions with respect to the polarization axis can be investigated by changing the polarization direction with respect to the direction of the detector. This method is called “mass resolved momentum imaging” (MRMI) [2]. By using the MRMI method, ultrashort structural deformation and the Coulomb explosion processes of polyatomic molecules such as CO_2 and NO_2 induced by an intense laser field were also investigated by this method [3, 4].

By adopting a method called “velocity map imaging” [5], with a position sensitive detector such as a MCP-Phosphor screen and a delay line detector, the momentum release of the generated ions can be recorded as a two-dimensional image. When a delay line detector is used, and the number of molecules ionized by one laser pulse is less than one, three dimensional momenta of all the fragment ions generated from a molecule can be determined by coincident detection. This method is called “coincidence momentum imaging (CMI)” [6], by which co-existing different fragmentation pathways can be investigated separately.

Through the CMI method, ultrafast migration processes of a hydrogen atom within a molecule induced by an intense laser field were identified [7-10]. Furthermore, a recent study on methyl-d_3 acetylene, D/H exchange process and hydrogen scrambling (D/H exchange and D migration) processes were identified [11].

1.3 Few-cycle pulses

In order to investigate ultrafast dynamics of molecules, we need to generate ultrashort laser pulses. The temporal shape of a laser pulse $E(t)$ and the spectral shape $E(\omega)$ are related to each other by the Fourier transformation:

$$E(t) = \frac{1}{2\pi} \int_{-\infty}^{\infty} E(\omega) \exp(i(\omega t + \phi(\omega)))\mathrm{d}\omega, \tag{1.1}$$

where $\phi(\omega)$ is a spectral phase. The product of the temporal width of the pulse Δt (usually defined by the FWHM of the temporal shape of the intensity) and the spectral width $\Delta\omega$ cannot become smaller than a certain constant value C, that is,

$$\Delta t \Delta\omega \geq C. \tag{1.2}$$

The constant is $C = 2.8$ when the pulse has a Gaussian shape. Due to this uncertainty, the spectral width need to be broader for generating shorter laser pulses.

In order to generate few-cycle laser pulses, the bandwidth of femtosecond laser pulses needs to be broadened by a method such as a self-phase modulation (SPM) process, and the associated phase dispersion must be compensated. There are several methods with which the spectral width can be broadened by SPM; (i) focusing the laser pulses into a silica plate, (ii) inducing filamentation [12, 13], and (iii) focusing the pulses into a hollow core fiber filled with rare gas. Especially, the hollow core fiber technique is one of the most efficient way to generate broad band pulses with high beam quality and high pulse energy. It was demonctrated that few-cycle pulses were obtained by compensating the phase dispersion of the broad band pulses generated by the hollow core fiber technique[14-16].

The temporal width ~ 5 fs of such few-cycle pulses is shorter than the period of molecular vibration. Therefore, a pump-probe measurement with few-cycle pulses can trace the early stages of laser induced nuclear displacement within a molecule, leading to its deformation and/or dissociation. Indeed, the dissociation processes of simple diatomic molecules such as N_2 and O_2 was probed in real time, and the electron localization processes were investigated [19].

Because a few-cycle pulse has only a few extrema in the electric field oscillation, tunneling ionization, which is expected to proceed only around the extrema of the electric field, may occur only a few times within the pulse duration. As a result, sequential ionization processes may not occur during the laser pulse duration and only non-sequential ionization processes could lead to the multiple ionization. The non-sequential ionization is induced when an electron ejected through the tunneling ionization comes back to the ion core and collides with it.

1.4 CEP of few-cycle pulses

A carrier-envelop phase (CEP) is one of the important parameters that characterizes few-cycle laser pulses. The CEP is a phase of the oscillation of the electric field within the envelop of the laser pule. For example, when the laser electric field has a Gaussian shape, the temporal electric field can be written with the CEP denoted as ϕ_{CEP} as

$$E(t) = E_0(t)\cos(\omega t + \phi_{CEP}), \tag{1.3}$$

where

$$E_0(t) = E_0 \exp\left(-\left(\frac{t}{\tau}\right)^2\right) \tag{1.4}$$

is a Gaussian envelope function which E_0 being the maximum amplitude. Figure 1.1 shows two examples of the few-cycle pulses. When CEP is 0 or π, the peak of the envelope coincides with the peak of the electric field, and the pulse becomes the cosine shape. When CEP is $\pi/2$ or $3\pi/2$, the pulse becomes the sine shape and the maximum amplitude of the electric field becomes the lowest. In the longer pulses in which the electric field

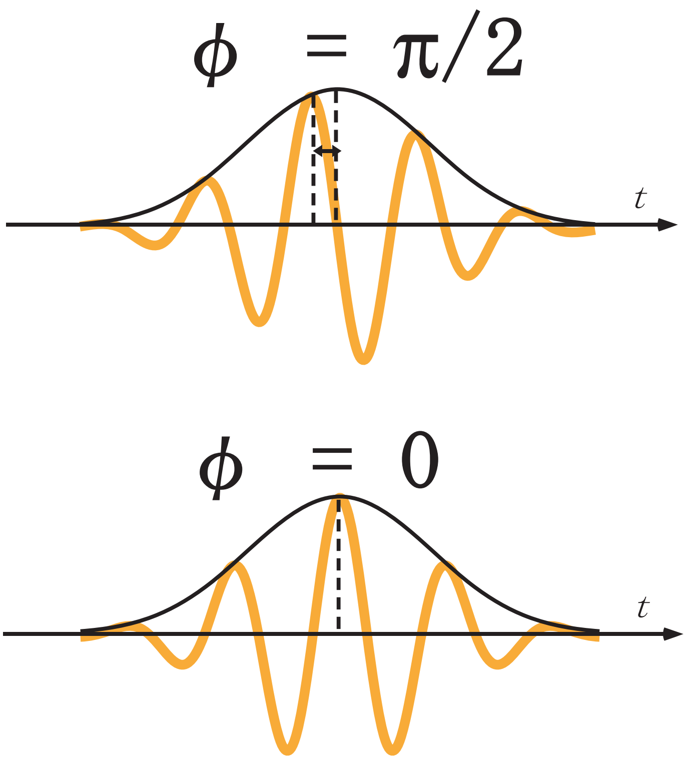

Fig 1.1: Few cycle pulse and CEP.

oscillate many times, the CEP may not be an important parameter characterizing the laser pulse. However, in the case of few-cycle pulses, the shape of the temporal electric filed varies significantly depending on the CEP. As a result, ultrafast dynamics of molecules induced by few-cycle laser pulses are expected to depend on their CEP.

When investigation of the CEP effect on ultrafast molecular dynamics, we need to know CEP of laser pulses employed in the experiment. A straightforward way is to lock the CEP of the pulse [20]. The CEP locking can be realized by controling the CEP offset of the spectrum of the pulses through manipulation of the laser oscillator conditions by changing the temperature of the laseing medium, the pulse energy of the pump laser, and the dispersion of the laser cavity.

Even when the CEP is not stabilized, if the CEP can be measured shot-by-shot, the

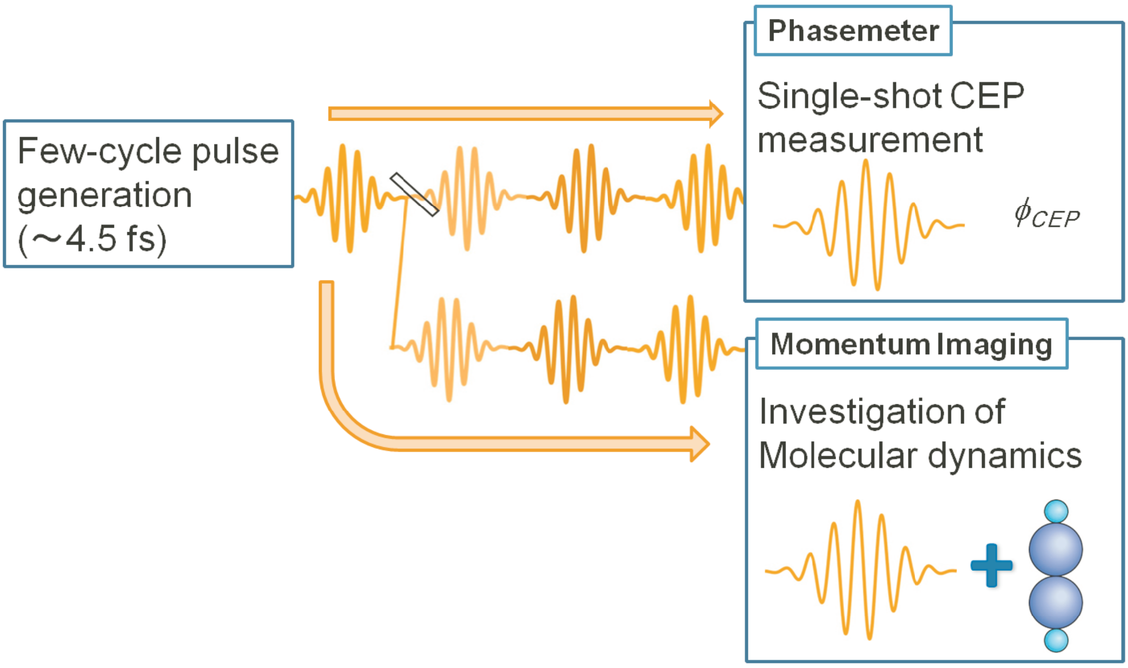

Fig 1.2: Schematics of the CEP-tagging experiment.

effect of the CEP can be investigated. Paulus *et al.* [17, 18] invented a "phasemeter", with which we can measure the CEP of each pulse by detecting simultaneously the photoelectron emission from rare gas atoms. In their experiment, few-cycle pulses were divided into two beams. One of the beams was introduced to the phasemeter to measure the CEP, and the other was used to induce ionization of atomic and molecular species [21] as shown in Fig.1.2. By the method called "CEP-tagging", in which the output signals of the phasemeter and the ion signals are recorded simultaneously so that their one-to-one correspondence is achieved, the CEP dependence can be investigated.

1.5 CEP dependent dynamics of atoms and molecules

The CEP dependences of atomic or molecular processes induced by few-cycle pulses have been reported in these several years [22-29]. In those studies, motion of electrons within a sub-cycle time scale was investigated.

Photoelectron emission from an atom is one of the examples of the CEP dependent processes. The photoelectron emission along the laser polarization direction becomes asymmetric depending on the CEP of the few-cycle pulse reflecting the asymmetry in the electric field and vector potential [22]. This asymmetry becomes salient in the above-threshold ionization (ATI) processes originating from the sub-cycle motion of the re-scattering electrons, and this asymmetry in ATI process is the operating principle of the phasemeter.

It was reported that the yield of ions generated through non-sequential double ionization (NSDI) process induced by few-cycle pulses varied depending on the CEP [21, 23, 24]. The variations of the ion yield were ascribed to the CEP dependent variation in the largest amplitude of the electric field of the few-cycle pulses. This type of CEP dependence exhibits the cycle with the period of π.

The effects of CEP on ionization and fragmentation dynamics of diatomic molecules have also been reported [25-28]. As for the study of the CEP effect on the homo-nuclear diatomic molecules, the CEP dependent dissociation of D_2 by the few-cycle pulses was investigated [25]. In those cases, the tunneling ionization rate and the molecular orbital are symmetric. The asymmetry was explained by the electron localization achieved by the subsequent electric field after the tunneling ionization [26]. This localization can be described theoretically by the coherent coupling of the 1sσ_g electronic ground state and the 2pσ_u electronic excited state of D_2^+.

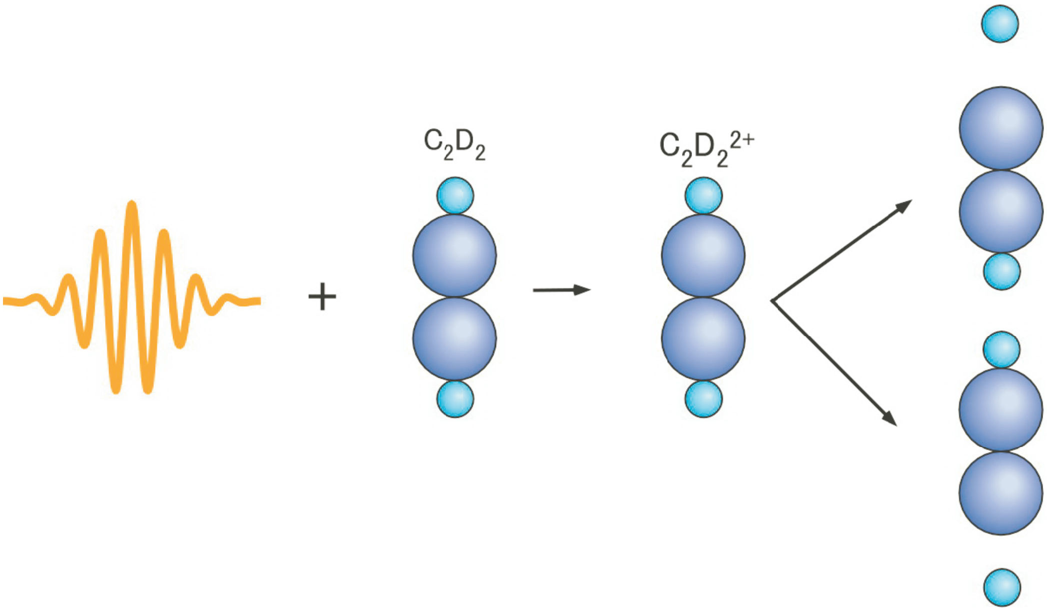

Fig 1.3: Asymmetry in D^+ emission from $C_2D_2^{2+}$ generated in a few-cycle laser pulse

1.6 Present study: CEP effect on the chemical bond breaking

In Chapter 3 of this thesis, the asymmetric dissociation of doubly charged deuterated acetylene $C_2D_2^{2+} \rightarrow C_2D^+ + D^+$, shown in Fig.1.3 induced by few-cycle pulses is studied by the CEP-tagging method using a phasemeter. An asymmetry was observed in the direction of the D^+ emission, and this asymmetry was found to vary depending on the CEP of the pulses. The origin of the CEP dependent asymmetry is discussed in view of ultrafast charge redistribution within $C_2D_2^2+$.

References

[1] D. Strickland and G. Mourou, *Opt. Commun.*, **56**, 219 (1985).

[2] A. Hishikawa, A. Iwamae, K. Hoshina, M. Kono and K. Yamanouchi, *Chem. Phys.*, **231**, 315 (1998).

[3] A. Hishikawa, A. Iwamae and K. Yamanouchi, *Phys. Rev. Lett.*, **83**, 1127 (1999).

[4] A. Hishikawa, A. Iwamae and K. Yamanouchi, *J. Chem. Phys.*, 111, 8871 (1999).

[5] A. T. J. B. Eppink and D. H. Parker, *Rev. Sci. Instrum.*, **68**, 3477 (1997).

[6] H. Hasegawa, A. Hishikawa and K. Yamanouchi, *Chem. Phys. Lett.*, **349**, 57 (2001).

[7] H. Hasegawa, A. Hishikawa and K. Yamanouchi, *J. Elec. Spec.*, **141**, 195 (2004).

[8] T. Okino, Y. Furukawa, P. Liu, T. Ichikawa, R. Itakura, K. Hoshina, K. Yamanouchi and H. Nakano, *Chem. Phys. Lett*, **419**, 213 (2006).

[9] T. Okino, Y. Furukawa, P. Liu, T. Ichikawa, R. Itakura, K. Hoshina, K. Yamanouchi and H. Nakano, *J. Phys. B: At. Mol. Opt. Phys.*, **39**, S515 (2006).

[10] H. Xu, C. Marceau, K. Nakai, T. Okino, S. L. Chin and K. Yamanouchi, *J. Chem. Phys.*, **133**, 071103 (2010).

[11] T. Okino, A. Watanabe, H. Xu and K. Yamanouchi, *Phys. Chem. Chem. Phys.*, **14**, 10640 (2012).

[12] C. P. Hauri, W. Kornelis, F. W. Helbing, A. Heinrich, A. Couairon, A. Mysyrowicz, J. Biegert and U. Keller, *Appl. Phys. B*, **79**, 673 (2004).

[13] S.A. Trushin, S. Panja, K. Kosma, W. E. Schmid and W. Fus, *Appl. Phys. B*, **80**, 399 (2005).

[14] M. Nisoli, S. De Silvestri and O. Svelto, *Appl. Phys. Lett.*, **60**, 2793 (1996).

[15] M. Nisoli, S. De Silvestri, O. Svelto, R. Szipöcs, K. Ferencz, Ch. Spielmann, S. Sartania and F. Krausz, *Opt. Lett.*, **22**, 522 (1997).

[16] M. Nisoli, S. Stagira, S. De Silvestri, O. Svelto, S. Sartania, Z. Cheng, M. Lenzner, Ch. Spielmann and F. Krausz, *Appl. Phys. B*, **65**, 189 (1997).

[17] G. G. Paulus, F. Lindner, H.Walther, A. Baltuska, E. Goulielmakis, M. Lezius and F. Krausz, *Phys. Rev. Lett.*, **91**, 253004 (2003).

[18] T. Wittmann, B. Horvath, W. Helml, M. G. Schatzel, X. Gu, A. L. Cavalieri, G. G. Paulus and R. Kienberger, *Nat. Phys.*, **5**, 357 (2009).

[19] I. A. Bocharova, A. S. Alnaser, U. Thumm, T. Niederhausen, D. Ray, C. L. Cocke and I. V. Litvinyuk *Phys. Rev. A*, **83**, 013417 (2011).

[20] D. J. Jones, S. A. Diddams, J. K. Ranka, A. Stentz, R. S. Windeler, J. L. Hall and S. T. Cundiff, *Science*, **288**, 635 (2000).

[21] N. G. Johnson, O. Herrwerth, A. Wirth, S. De, I. Ben-Itzhak, M. Lezius, B. Bergues, M. F. Kling, A. Senftleben, C. D. Schröter, R. Moshammer, J. Ullrich, K. J. Betsch, R. R. Jones, A. M. Sayler, T. Rathje, K. Rühle, W. Müller and G. G. Paulus, *Phys. Rev. A*, **83**, 013412 (2011).

[22] S. Chelkowski and A. D. Bandrauk *Phys. Rev. A*, **71**, 053815 (2005).

[23] S. Micheau, Z. Chen, Anh-Thu Le and C. D. Lin, *Phys. Rev. A*, **79**, 013417 (2009).

[24] X. Xie, K. Doblhoff-Dier, S. Roither, M. S. Schöffler, D. Kartashov, H. Xu, T. Rathje, G. G. Paulus, A. Baltuska, S. Gräfe and M. Kitzler, *Phys. Rev. Lett.*, **109**, 243001 (2012).

[25] M. F. Kling, Ch. Siedschlag, A. J. Verhoef, J. I. Khan, M. Schultze, Th. Uphues, Y. Ni, M. Uiberacker, M. Drescher, F. Krausz and M. J. J. Vrakking, *Science*, **312**, 246 (2006).

[26] P. von den Hoff, I. Znakovskaya, M. F. Kling and R. de Vivie-Riedle, *Chem. Phys.*, **366**, 139 (2009).

[27] I. Znakovskaya, P. von den Hoff, S. Zherebtsov, A. Wirth, O. Herrwerth, M. J. J. Vrakking, R. de Vivie-Riedle and M. F. Kling, *Phys. Rev. Lett.*, **103**, 103002 (2009).

[28] I. Znakovskaya, P. von den Hoff, N. Schirmel, G. Urbasch, S. Zherebtsov, B. Bergues, R. de Vivie-Riedle, K.-M. Weitzel and M. F. Kling, *Phys. Chem. Chem. Phys.*, **13**, 8653 (2011).

[29] F. Krausz and M. Ivanov, *Rev. Mod. Phys.*, **81**, 163 (2009).

Chapter 2. Experimental setup for few-cycle pulse experiment

2.1 Introduction

Historically, the CEP effects on the atomic or molecular dynamics were investigated by CEP locked laser systems [1, 2]. Through the studies of the CEP dependent photo-electron emission from atoms, the technique to measure the CEP of the few-cycle pulses has been developed. Wittman $et\ al.$ succeeded in a single-shot measurement of the CEP of the few-cycle pulses with random phases [3], and the newly invented apparatus called phasemeter enabled us to investigate the CEP effects on the atomic or molecular dynamics without locking the CEP of the pulses.

In the present study, a new experimental setup for investigating the CEP dependent molecular dynamics was constructed by taking advantage of the CEP tagging method. The overview of the experimental setup is shown in Fig. 2.1. From the output of a Ti:Sapphire laser system, few-cycle pulses are generated by using a homemade hollow-core fiber pulse compressor. The CEP of the pulses are characterized by a phasemeter developed by Prof. G. Paulus at Friedrich-Schiller-Universität, Jena. Ion species generated by the irradiation of few-cycle pulses are measured by a momentum imaging chamber. The data from the two apparatuses are simultaneously recorded in coincidence by a time-to-digital converter (TDC8HP) and thus the CEP dependences of the yields and momentum vectors of the ions are recorded.

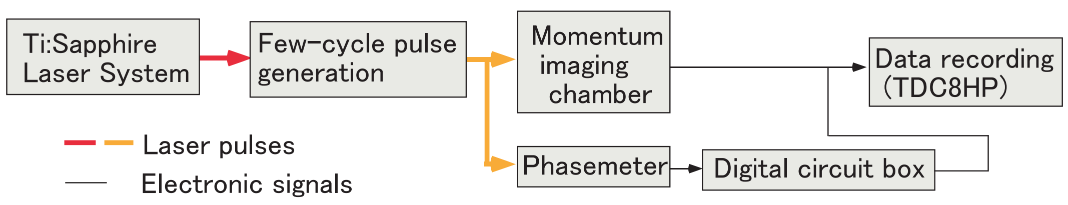

Fig 2.1: Overview of the experimental setup.

2.2 Laser system Alpha 5000

The laser system used in the present study is Alpha/XS manufactured by THALES LASER. Co. Ltd. The schematics of the system is shown in Fig. 2.2. The Ti:Sapphire oscillator RAINBOW (FEMTOLASERS Produktions GmbH.) is pumped by a cw 532 nm output of Nd:YVO_4 green laser (Verdi, Coherent Inc.). The repetition rate of the the oscillator output is 78 MHz and the power is typically 160 mW. The pulse duration of ultrashort pulses from the oscillator is stretched to $\sim$100 ps by an Öffner type grating stretcher [4]. The spectral intensity and the spectral phase of the stretched pulses are modulated by an acousto optic modulator (Dazzler, FASTLITE). The modulated pulses are amplified up to 0.7 mJ/pulse by a regenerative amplifier and a two-pass amplifier. The output of a green laser ETNA (THALES LASER. Co. Ltd, 532 nm, 5 kHz) are used for the amplification. The repetition rate of the pulses are reduced to 5 kHz by this amplification process. The amplified pulses are compressed by a Treacy type grating compressor, and the pulse width of the output pulses typically are 30 fs at the Fourier transform limit as shown in the autocorrelation trace measured by our group (Fig. 2.3).

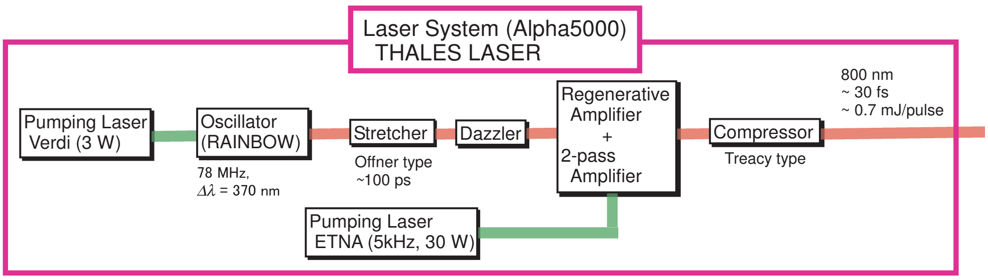

Fig 2.2: The schematic of the laser system used in the present study

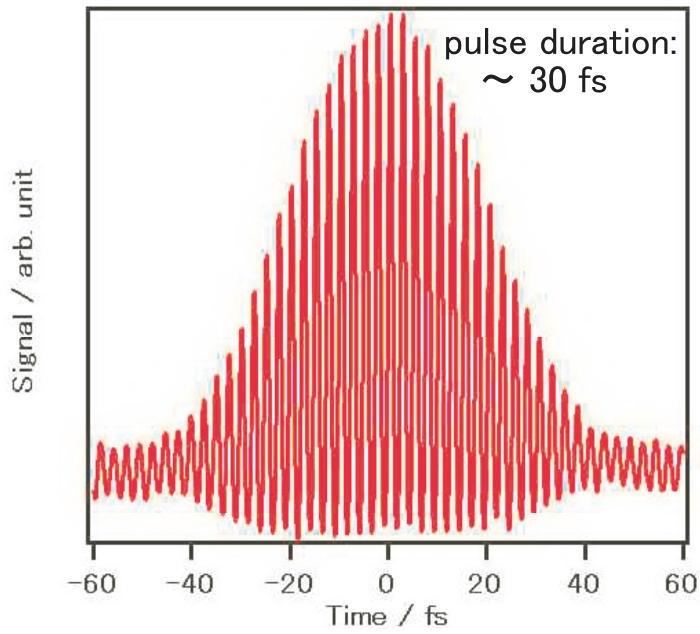

Fig 2.3: Autocorrelation trace of the output from the laser system. The pulse duration is about 30 fs.

2.3 Pulse compression by a rare-gas filled hollow-core fiber

2.3.1 Theory

Few-cycle pulses are generated by broadening the spectral width of the output pulses of the CPA Ti:Sapphire laser system and compensating the phase dispersion [5, 6]. For the broadening of the spectral width, a nonlinear process called self phase modulation is often used. When the field intensity of the laser pulse I becomes larger, the refractive index n of a medium increases, as

$$n = n_0 + n_2 I(t). \tag{2.1}$$

The coefficient n_2 is the nonlinear index coefficient and $n_2 = 9.8 \times 10^{-24}$ m^2/W [6] for 1 atm Ar gases. When the pulse propagates the length l in the medium, the phase shift $\Delta\phi$

can be expressed as

$$\Delta\phi = -\frac{2\pi n_2 l I(t)}{\lambda}, \tag{2.2}$$

where λ is the wavelength of the pulse. From the Eq.(2.2), the variation in the frequency at time t is expressed as

$$\Delta\omega(t) = -\frac{2\pi n_2 l}{\lambda}\frac{\mathrm{d}I(t)}{\mathrm{d}t}. \tag{2.3}$$

This equation means that, the frequency decreases at the rising part of the pulse, while the frequency increases in the falling part of the pulse. Thus, propagation of the intense laser pulses in a nonlinear medium causes the broadening of the spectrum.

2.3.2 Experimental and results

A schematic of the setup of few-cycle pulse generation is shown in Fig.2.4. For the generation of few-cycle pulses, the spectral width of the pulses is broadened by focusing the femtosecond pulses into a hollow-core fiber filled with an Ar gas. In the present study, in order to reduce the number of transmission optics, a concave mirror is used to focus the pulses into the hollow-core fiber instead of a lens. The hollow-core fiber compressor is composed of a hollow-core fiber (length 1.5 m, inner diameter 330 μm), a V-groove mount and a stainless tube. The entrance and the exit of the tube are mounted on xyz three-axis stages respectively for fine alignment of the fiber.

The laser pointing of the focus position are stabilized by a computer controlled stabilization system(Aligna 4D,TEM Messtechnik) composed of two steering mirrors mounted on piezo driven mirror mounts and a concave mirror. The laser pointing and the position of the laser focus are monitored and stabilized using two position sensitive detectors. The focal length of the concave mirror which focus the laser pulses into the hollow-core fiber is 1.5 m, and the focal diameter is ~220 μm. When the Ar gas pressure is 0.47 atm, the

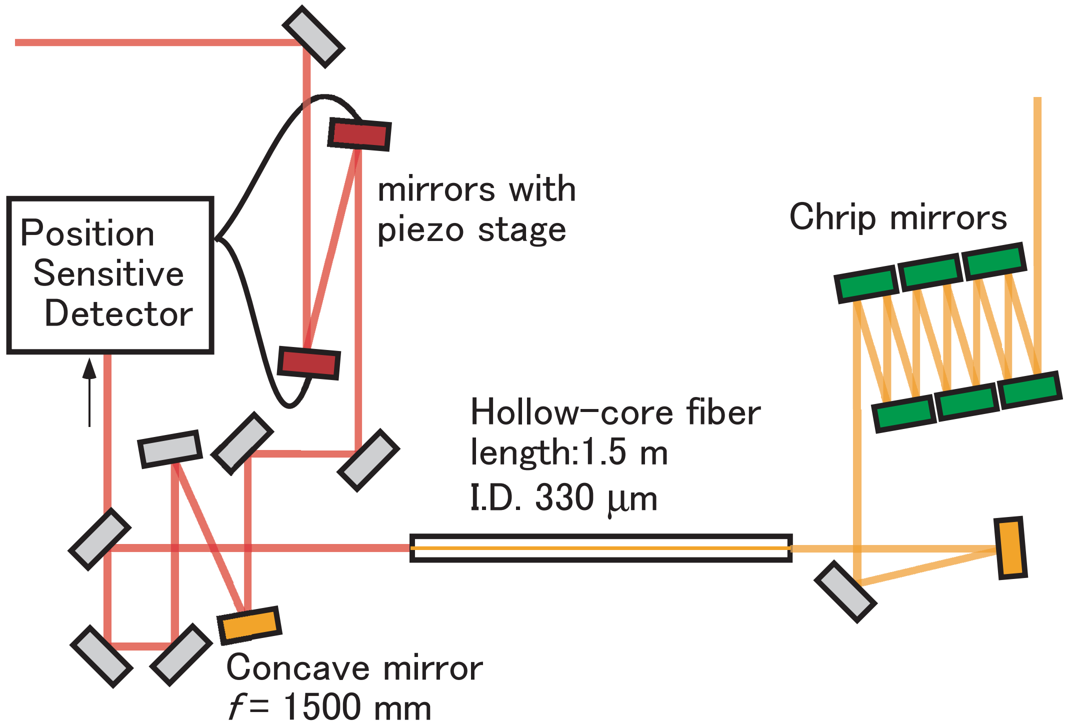

Fig 2.4: The setup for few-cycle pulse generation

full-width of the tenth-maximum is about 350 nm as shown in the spectrum of the output from the hollow-core fiber shown in Fig.2.5.

The phase dispersion of the pulse is compensated by a set of chirp mirrors (BB-COMP). Figure 2.6 shows an auto-correlation trace of the compressed pulse showing that the pulse width becomes as short as $\sim$ 5 fs after the compression.

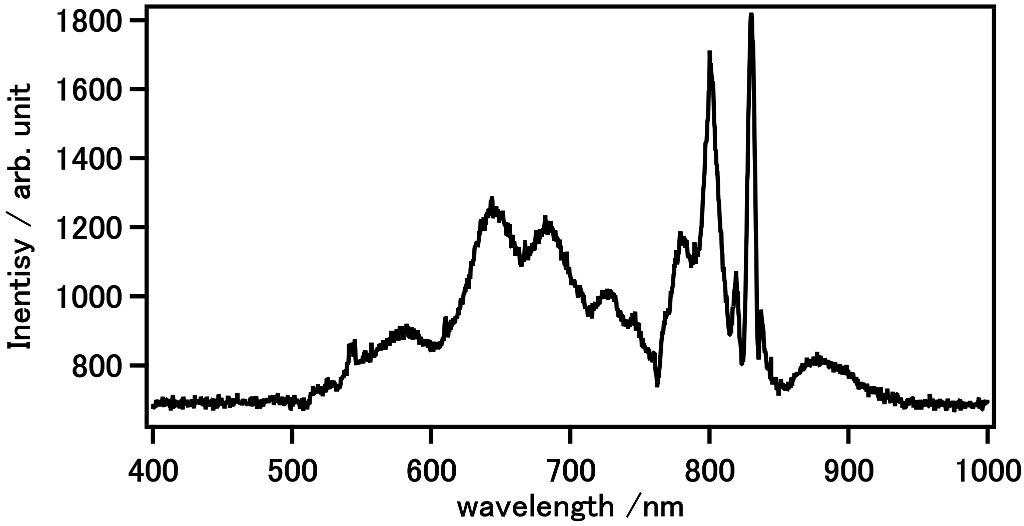

Fig 2.5: Spectrum of the output from the hollow-core fiber.

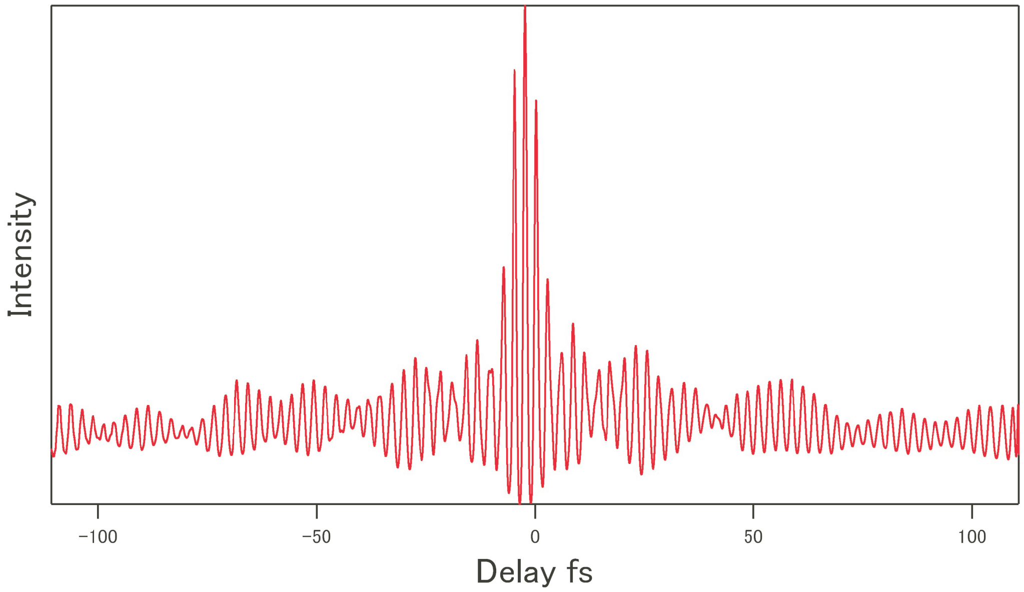

Fig 2.6: Auto-correlation trace of the generated puleses. The pulse width is estimated to be ∼5 fs.

2.4 Carrier envelope phasemeter

2.4.1 Overview

A phasemeter is an apparatus with which we measure the CEP of a few-cycle pulse by detecting the asymmetry of photoelectron emission direction from rare gas atoms. A schematic of a phasemeter is shown in Fig.2.7. A phasemeter is composed of a cell where rare gases are filled, two slits from which photoelectron can be emitted, and two MCP detectors placed on both ends of the tube for electrons. Both of the photoelectron spectra recorded using the two MCP detectors are divided into two energy regions, that is, the higher energy region and the lower energy region. By plotting the asymmetry of the photoelectron signal in the respective energy regions shot-by-shot, a two dimensional map called a parametric asymmetry plot is obtained. The relative CEP of a pulse represented by a point in the plot can be estimated from the angle of the point in the polar coordinate system and this plot becomes round-shaped when the CEP of the output pulses are not stabilized.

2.4.2 Experimental and results

The few-cycle pulses are divided into two beams by a beam splitter. The reflection at the beam splitter is introduced into the phasemeter. The polarization of the pulses is rotated by 90 degrees by a periscope so that the polarization of the pulse becomes horizontal. The pulses are focused by a concave mirror (f = 250 mm) into the chamber where a Xe gas is filled, and the emitted photoelectrons are detected by the two MCP detectors. Detection of low-energy electrons is avoided by applying retardation voltage (-25 V) just before the detectors, and thus, only high-energy photoelectrons emittied through high-order ATI process are selectively detected. Hereafter, the the signal intensities in

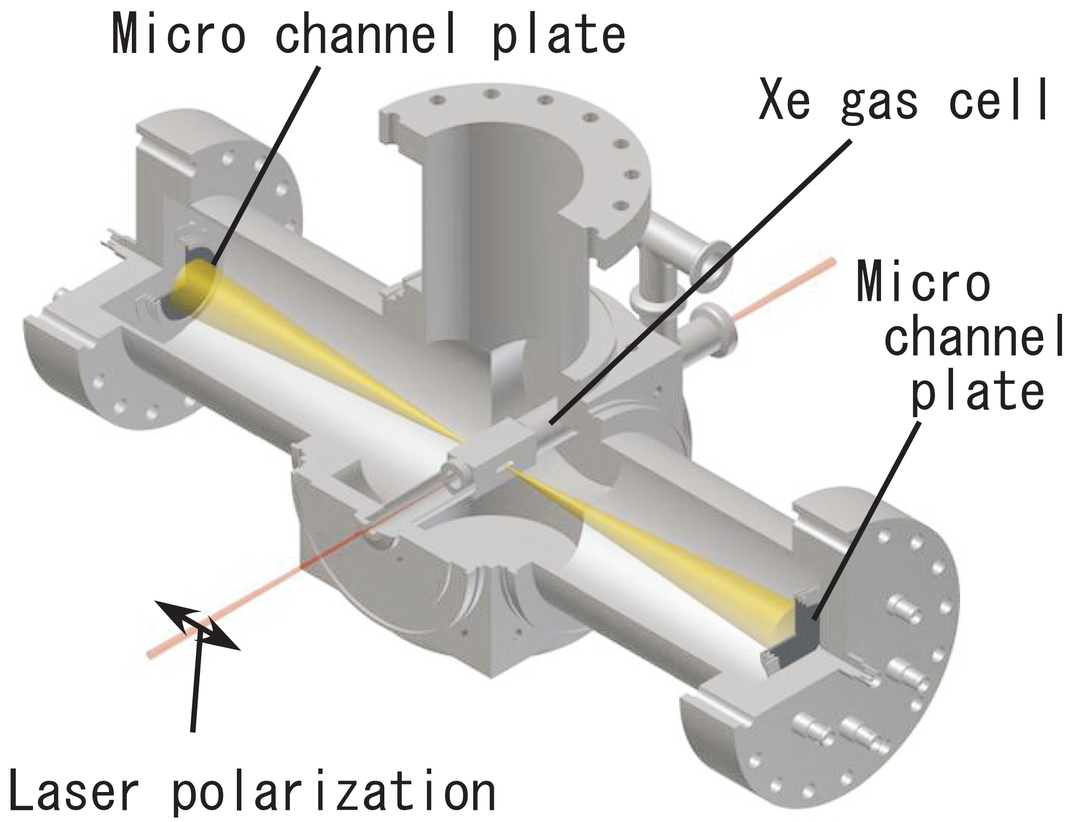

Fig 2.7: Phasemeter.

the photoelectron spectrum in the lower and higher energy regions detected by the right side detector are denoted as $I_{\text{low,right}}$, $I_{\text{high,right}}$ and those detected by the left side detector are denoted as $I_{\text{low,left}}$, $I_{\text{high,left}}$. Then, the asymmetry of the photoelectron emission $P_{\text{asym,low}}$, $P_{\text{asym,high}}$ are defined as

$$P_{\text{asym,low}} = \frac{I_{\text{low,left}} - I_{\text{low,right}}}{I_{\text{low,left}} + I_{\text{low,right}}} \tag{2.4}$$

and

$$P_{\text{asym,high}} = \frac{I_{\text{high,left}} - I_{\text{high,right}}}{I_{\text{high,left}} + I_{\text{high,right}}}. \tag{2.5}$$

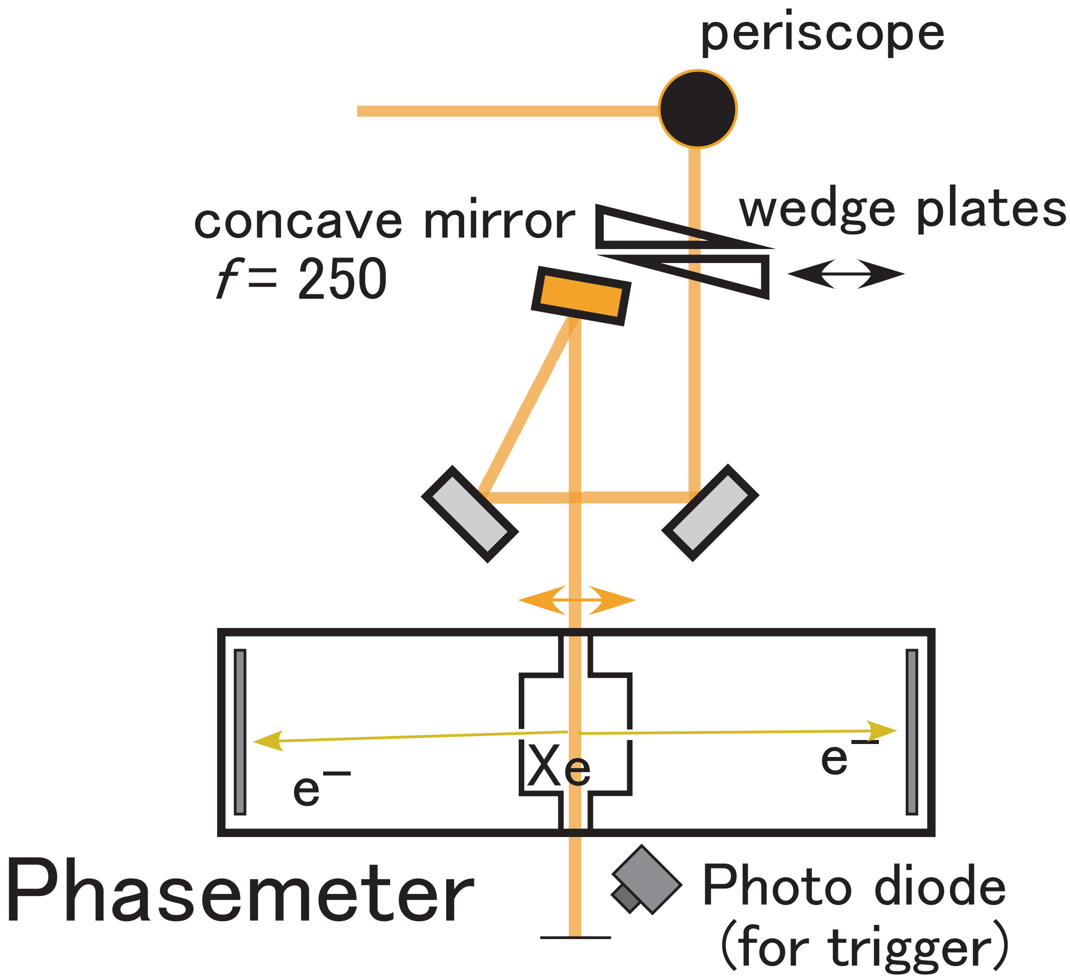

Fig 2.8: Setup for CEP measurement.

The signals are entered into a digital circuit by which the asymmetry parameters calculated as explained in Section 2.7. When $P_{\text{asym,high}}$ is plotted with respect to $P_{\text{asym,low}}$, a map called a parametric asymmetry plot is obtained. The polar angle of the respective points in the plot represents the relative CEP of the pulse. On the other hand, the radius of the points represents the pulse duration. When the pulse duration become shorter the radius becomes larger. Thus, the pulse duration of the pulses can be estimated from the plot. The Ar gas pressure in the hollow-core fiber and the extent of the insertion of the wedge plates are adjusted so that the radius of an asymmetry plot becomes largest. Figure

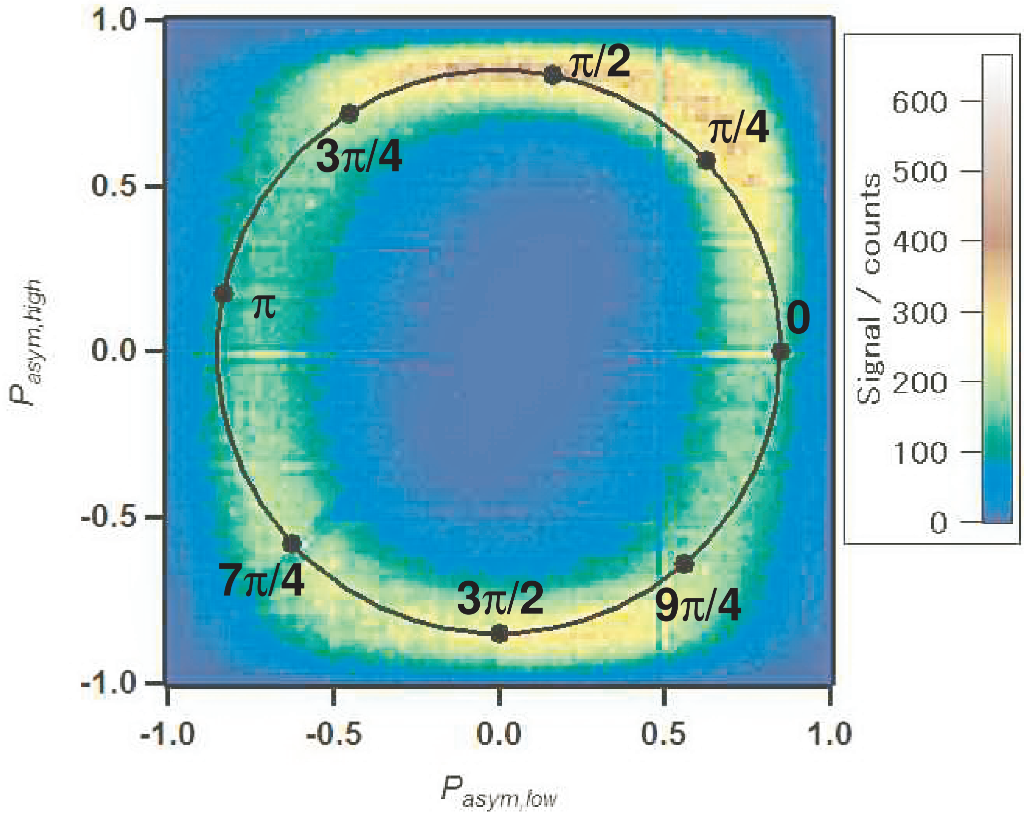

Fig 2.9: A parametric asymmetry plot. The radius of the plot is ∼0.8.

2.9 shows a typical parametric asymmetry plot. From the figure, the pulse duration is estimated to be ∼4.5 fs.

2.5 Momentum imaging chamber

2.5.1 Overview

The detection of the generated ions are performed using a momentum imaging chamber. The drawing of the chamber is shown in Fig. 2.10. In the chamber, laser pulses are focused on a beam of a molecular sample gas. The ions generated through the interaction of laser pulses and the sample gases are extracted by a static electric field and are guided to a position sensitive detector. From the time-of-flight of the ions and the positions on

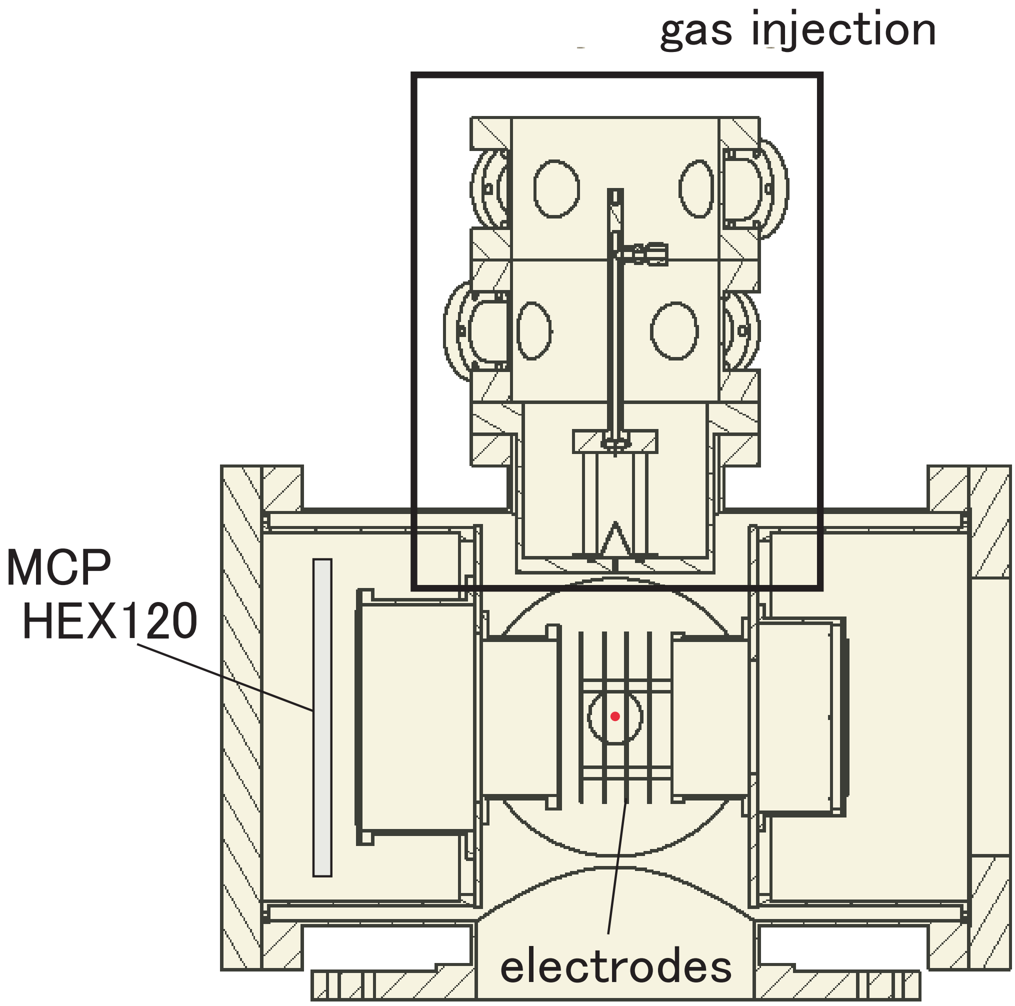

Fig 2.10: Drawing of the momentum imaging chamber.

the detector, three-dimensional momentum vectors of the ions are determined.

2.5.2 Gas injection

A diffusive molecular beam of a sample gas is introduced from a microsyringe into the chamber through a skimmer as shown in Fig. 2.11. The diameter of the hole at the tip of the skimmer is 0.4 mm. From the geometric configuration, the width of the molecular beam at the interaction region with laser pulses is estimated to be $\sim$1.5 mm.

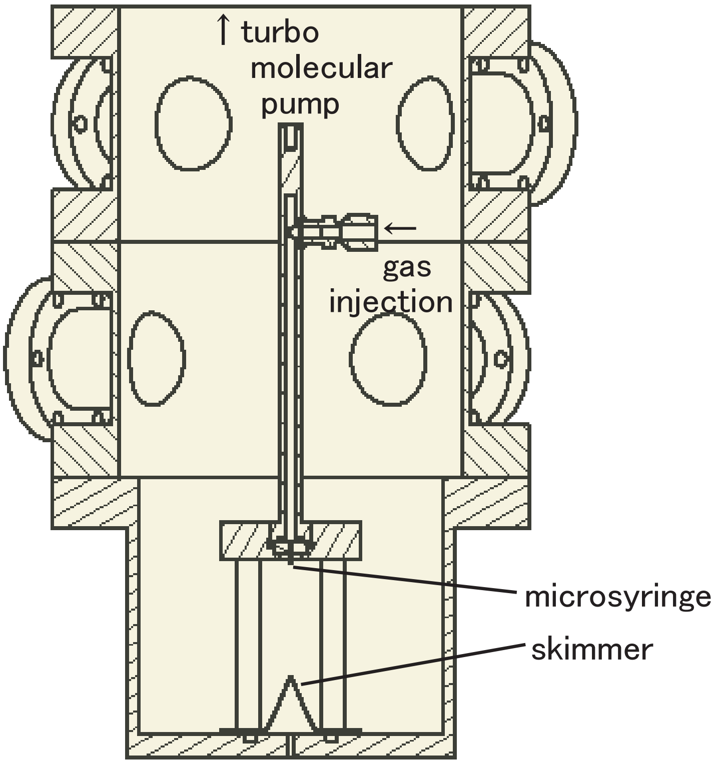

Fig 2.11: Drawing of the gas injection part of the momentum imaging chamber.

2.5.3 Ion extraction

For the ion extraction, three electrodes are fixed in the both sides of the interaction region, respectively. The ions are accelerated by the static electric field created by applying dc voltages to the four electrodes as shown in Fig. 2.12. From the detection position and the time-of-flight of the detected ions, the three-dimensional momentum release of the detected ions can be determined.

The initial distribution of the position of the generated ions in the direction perpendicular to the TOF axis mainly results in the decrease of the resolution of the detecting position. In the momentum imaging chamber, static electric fields create a lens for ions, and therefore the trajectories of the generated ions can be focused onto the detector. If we

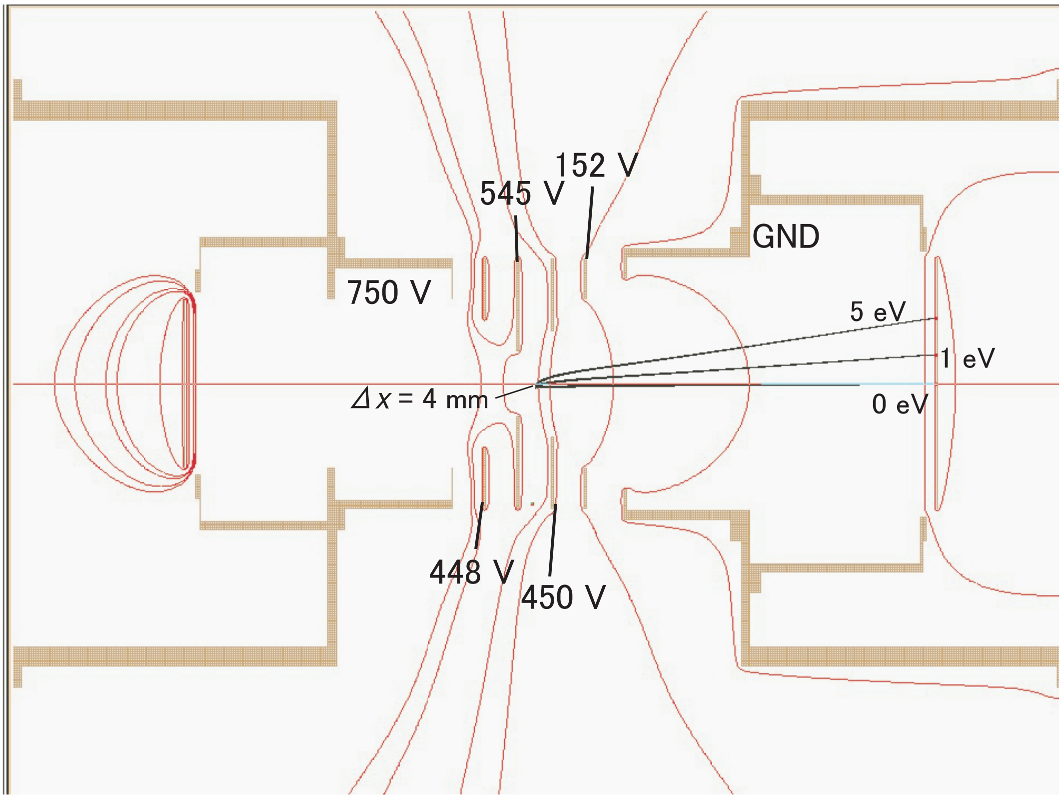

Fig 2.12: Focusing voltage condition of the ion trajectories.

can cancel the initial position distribution, the detection position corresponds to the initial velocity or momentum of the ions. This is called the velocity map imaging condition [8].

In the present study, trajectories of the ions are simulated by SIMION, and the optimum voltage conditions are found so that the velocity map imaging condition is fulfilled. The geometric configuration of the electrodes in the chamber, the voltage conditions and the trajectories of H^+ with the 0 eV, 1 eV, and 5 eV kinetic energies are shown in Fig.2.12.

2.5.4 Ion detection

For the ion detection, a position sensitive detector HEX120 (Roentdek Handels GmbH.) composed of two MCPs with chevron stacking and delay-line wires is used. When an ion hit on the surface of the MCP detector, secondary electrons are generated and the signals are amplified. At the rear side of the MCP plates, three delay line wires are mounted in a helical shape. The electron signals hit on the wires induces the electric signal which propagates to both side of the wires. The timing of the signal arrivals are recorded by a digital board TDC8HP (Roentdek Handels GmbH.).

The procedure to derive the position of the detection from the six signals ($x_1, x_2, y_1, y_2, z_1, z_2$) are as follows. As the difference between the two arrival timings at the both end of one wire corresponds to the position in the coordinate, and from the three sets of the data

$$
\begin{aligned}
u &= (x_1 - x_2)V_u/2 && (2.6)\\
v &= (y_1 - y_2)V_v/2 && (2.7)\\
w &= (z_1 - z_2)V_w/2, && (2.8)
\end{aligned}
$$

are obtained, where $V_\mathrm{u}, V_\mathrm{v}, V_\mathrm{w}$ are the speed of the electric signal propagation in the wires. The speeds are slightly different by the wire as described in the next subsection. From two values of the hexagonal coordinate, 2-dimensional position is reconstructed:

$$
\begin{aligned}
X_{uv} &= u && (2.9)\\
Y_{uv} &= \frac{1}{\sqrt{3}}(u - 2v) && (2.10)\\
X_{uw} &= u && (2.11)\\
Y_{uw} &= \frac{1}{\sqrt{3}}(2w - u) && (2.12)\\
X_{vw} &= v + w && (2.13)\\
Y_{vw} &= \frac{1}{\sqrt{3}}(w - v) && (2.14)
\end{aligned}
$$

Theoretically, $(X_{uv}, Y_{uv}), (X_{uw}, Y_{uw}), (X_{vw}, Y_{vw})$ must be the same values.

2.5.5 Measurement of the signal propagation speed in the delay line wires

When the three values of X, Y are the same,

$$u = v + w \tag{2.15}$$

holds. Thus the relationship

$$x_1 - x_2 = \frac{V_\mathrm{v}}{V_\mathrm{u}}(y_1 - y_2) + \frac{V_\mathrm{w}}{V_\mathrm{u}}(z_1 - z_2) \tag{2.16}$$

can be derived. From the equation, the relative values V_v/V_u and V_w/V_u can be obtained from an experimental data. In order to determine the relative values V_v/V_u and V_w/V_u experimentally, ion signals from residual gases in the chamber are accumulated. Figure 2.13 shows the ($x_1 - x_2$) values plotted to ($y_1 - y_2$) and ($z_1 - z_2$). By the 2-dimensional fitting, the following ratios are obtained:

$$\frac{V_\mathrm{v}}{V_\mathrm{u}} = 1.0065 \pm 0.00135 \tag{2.17}$$

$$\frac{V_\mathrm{w}}{V_\mathrm{u}} = 1.0174 \pm 0.00135 \tag{2.18}$$

These ratios are used in the analysis of the data recorded by the detector.

If the static electric fields between the electrodes are uniform, the three dimensional momentum release (p_x, p_y, p_z) can be derived as:

$$p_x = \frac{mX}{T} \tag{2.19}$$

$$p_y = \frac{mY}{T} \tag{2.20}$$

$$p_z = ZeE(T - T_0) \tag{2.21}$$

where, X, Y is the detection position, m is the mass of the ion, T is the time of flight of the ion, T_0 is the central time of flight of the ion specie, and Ze is the charge of the ion. In

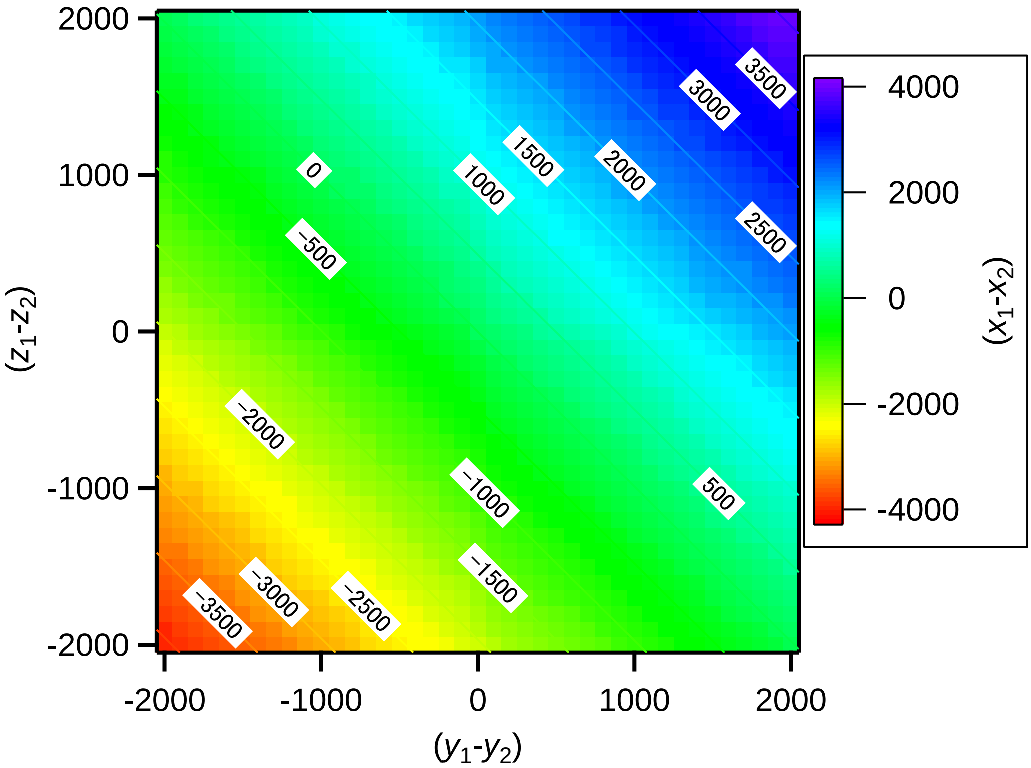

Fig 2.13: $(x_1 - x_2)$ values plotted to $(y_1 - y_2)$ and $(z_1 - z_2)$.

the momentum imaging chamber, the electric fields are not uniform and some corrections to the equations are needed.

The relationships between the detection position and the momentum of ions can be obtained by a SIMION simulation. A total of 441 trajectories of protons (hydrogen ions) with -50 $\times 10^3$ u m/s $\sim$ 50 $\times 10^3$ u m/s (21 points) for the momentum in the directions parallel and perpendicular to the time-of-flight axis are calculated. The initial momenta of a proton are indicated by the "+" marks in Fig. 2.14. From the position of the detection and time-of-flight, the following relations of the time of flight t (μs), the detection position x (mm) and the momentum (p_x, p_y, p_z) (10^3 u m/s) are obtained by a least-squares fits:

$$p_z(m = 1, t, x) \quad = \quad (-583.5 \pm 0.4)t + (-0.0157 \pm 0.0004)x^2 t$$

$$+(773 \pm 4)t^2 \tag{2.22}$$

$$p_{x,y}(m=1,t,x) = (0.9993 \pm 0.0003)x$$

$$+(-0.138 \pm 0.004)xt + (12.01 \pm 0.08)xt^2. \tag{2.23}$$

For heavier ions having the mass m, the corresponding equations can be obtained from Eqs (2.22) and (2.23) as

$$p_z(m,t,x) = \sqrt{m}p_z(m=1,\frac{t}{\sqrt{m}},x) \tag{2.24}$$

$$p_{x,y}(m,t,x) = \sqrt{m}p_{x,y}(m=1,\frac{t}{\sqrt{m}},x) \tag{2.25}$$

The momenta p'_x, p'_z converted from the simulation data t and x of the protons are indicated by the "+" marks in Fig. 2.15. The comparison between From Figs. 2.14 and 2.15 shows that the resultant momenta p'_x, p'_z agree well with the initial momenta p_x, p_z.

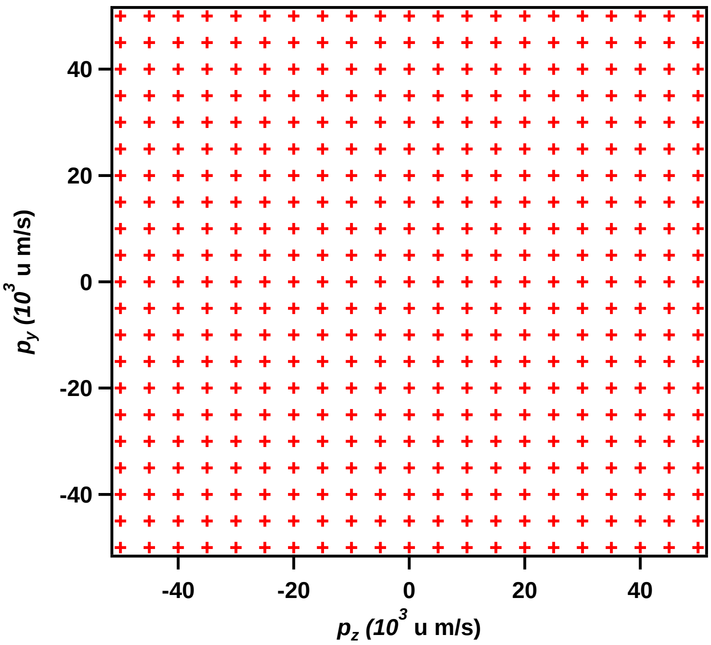

Fig 2.14: Initial momenta (p_x, p_z) of protons in the simulation

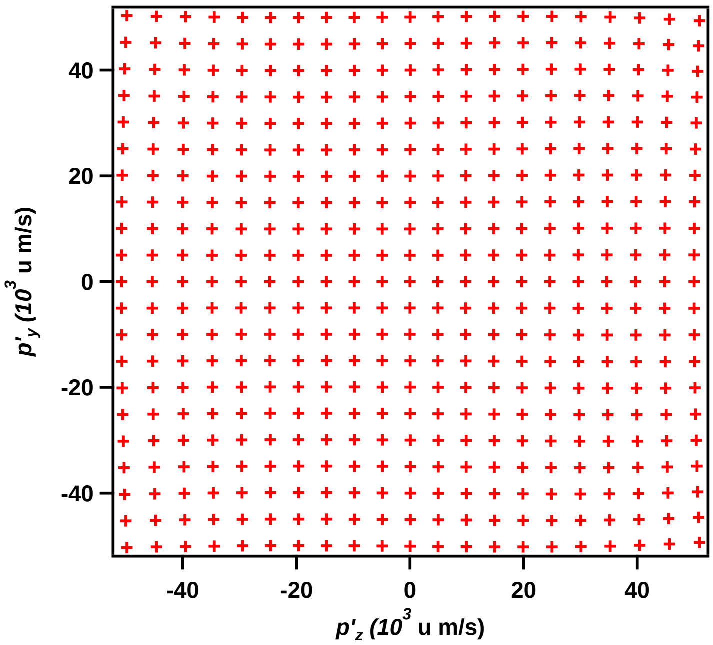

Fig 2.15: Momenta (p'_x, p'_z) of protons converted from the detection position and the time of flight.

2.5.6 Further improvement of the chamber

Figure 2.16 shows the histogram of the signals from the fragment ions generated from methanol (CH_3OH) with the time-of-flight as the horizontal axis and the Y position on the detection as the vertical axis. The range of the time-of-flight shown in this figure corresponds to $m/z = 14 \sim 18$. The observation can be explained by a simulation by SIMION, in which fragment ions with the kinetic energy of 3 eV are ejected in every direction from the position of the ionization, as shown in Fig. 2.17 . It can be seen in this figure that the signals of the ions having the adjacent m/z values overlap each other. In order to separate more these contributions from the different mass species, the length of the flight tube of the chamber is to be made longer. The mass separations were calculated when the length of the flight tube was assumed to be stretched by 20 cm to 39 cm, while keeping the VMI voltage conditions. The simulation shows that the extent of the overlap of the neighboring mass species is reduced and the signals of $m/z = 15$ can now be separated completely from that of $m/z = 17$ as shown in Fig. 2.19. In order to realize the longer flight tube in the experiment, several new parts is designed to improve the experimental chamber.

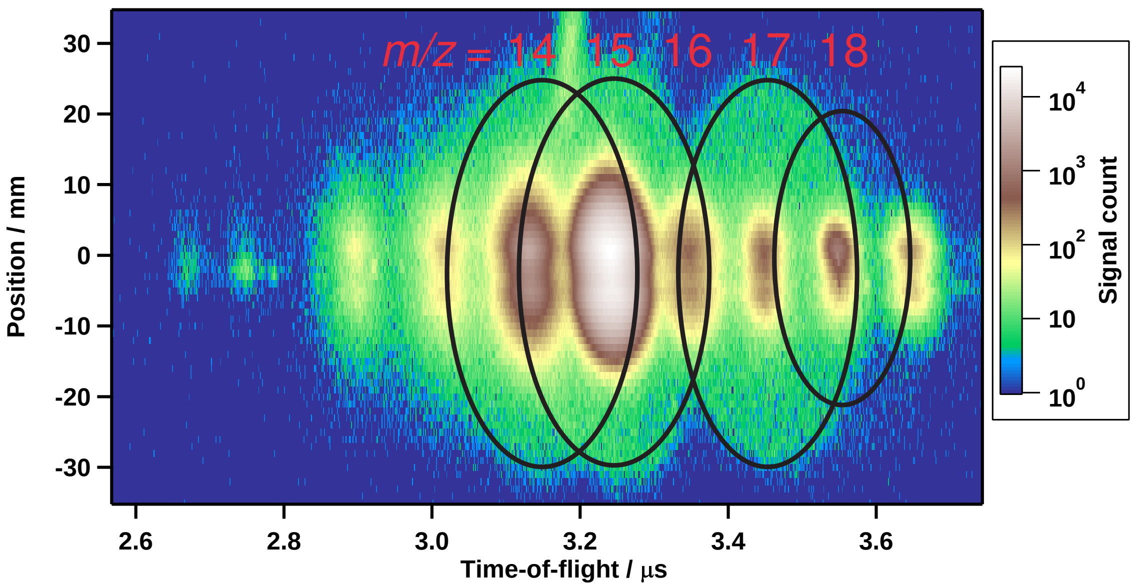

Fig 2.16: Histogram of the time-of-flight signals of fragment ions from methanol.

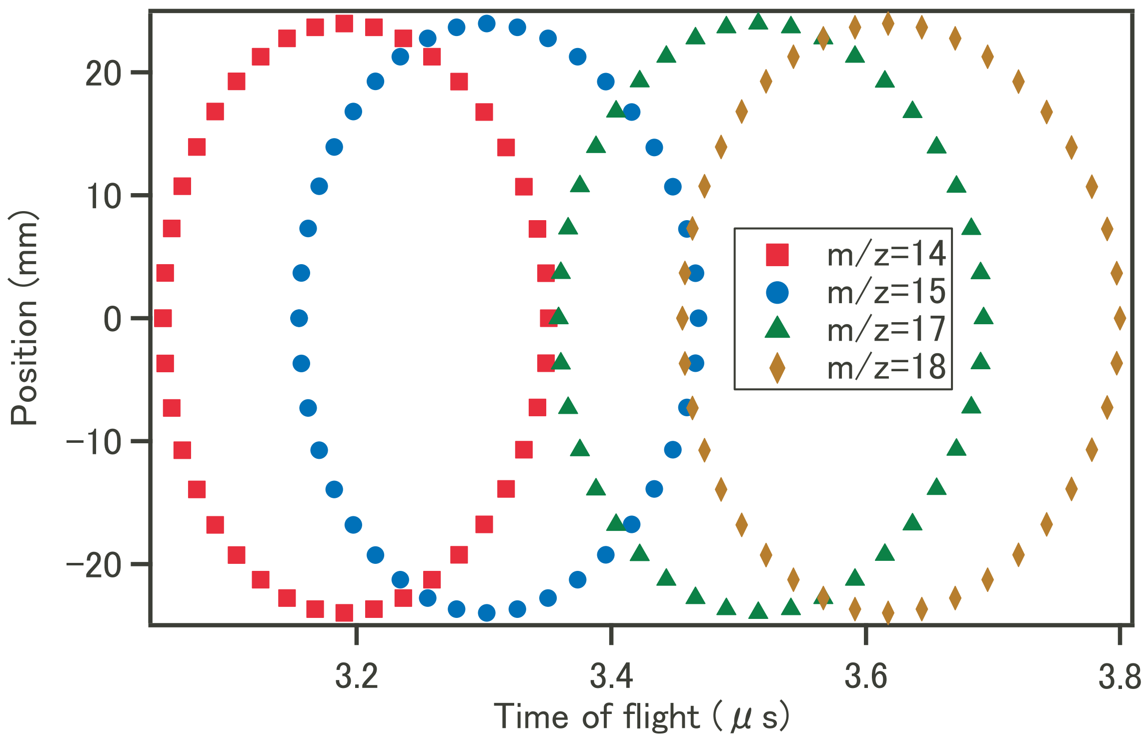

Fig 2.17: Time-of-flight and the detection position of the fragment ions having the kinetic energy of 3 eV. The azimuthal angle of the ejection direction of the ions are varied with 9-degree step.

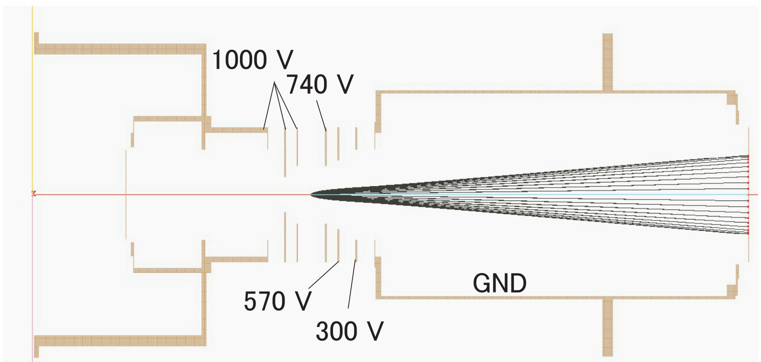

Fig 2.18: Configuration of the electrodes and the flight tube in the simulation for the longer chamber.

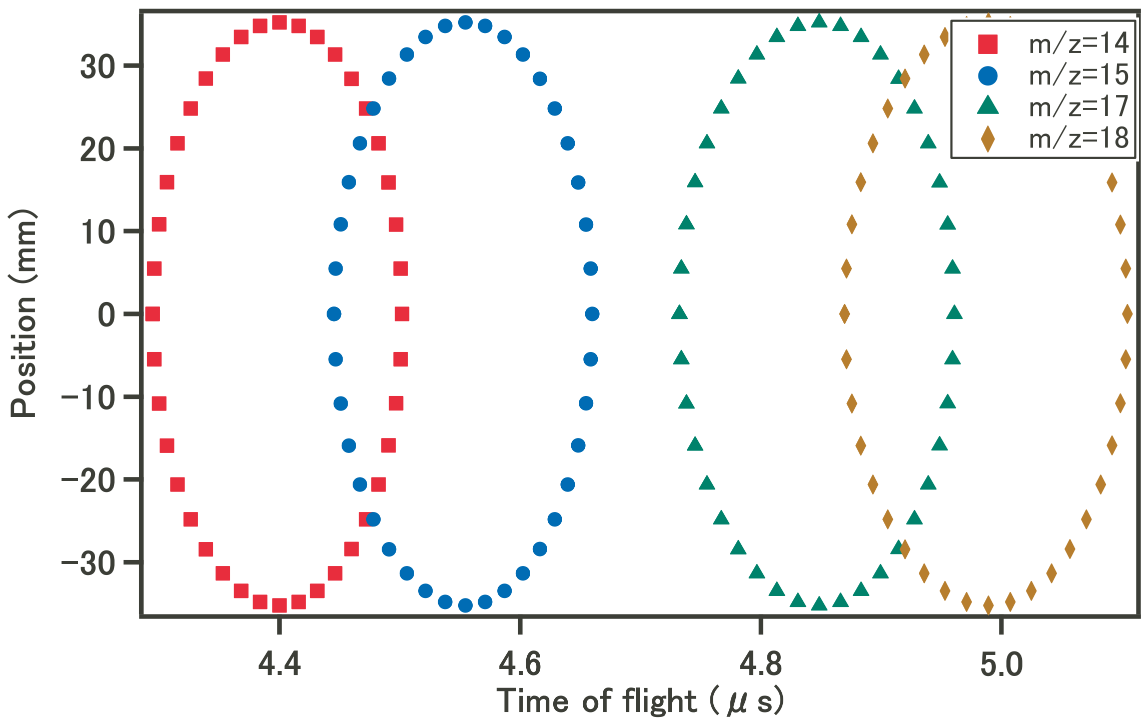

Fig 2.19: Same as in Fig. 2.17 but for the longer chamber and the new voltage conditions.

2.6 Synchronized measurement of the phasemeter and momentum imaging chamber

2.6.1 Overview

For the CEP-tagging measurement, the data from the phasemeter and the data from the momentum imaging chamber need to be recorded shot-by-shot in coincidence. The data from the momentum imaging chamber is recorded by the TDC8HP board. For the tagging measurement, asymmetry data from the phasemeter need also to be saved shot-by-shot. Here, a few methods to synchronize the measurements are tried.

2.6.2 Voltage to time converter

The photoelectron spectra recorded by the phasemeter are converted into a voltage output proportional to the asymmetry parameter by an analog circuit box, and its output is converted into the timing signal by a homemade voltage-to-time converter so that this timing signal representing the asymmetry parameter is entered into the TDC8HP simultaneously with the data from the momentum imaging chamber for the synchronization of the data acquisition from the two apparatuses.

2.6.3 Digital phasemeter box

In the measurements below, the conversion of the signals from the phasemeter are processed by a digital phasemeter developed by Friedrich-Schiller-Universität, Jena shown in Fig.2.20. The digital box calculates the asymmetry of the photoelectron spectra and converts the asymmetry data to a timing signal which can be directly recorded by the TDC8HP. The timing signal is put into the TDC8HP board and thus the simultaneous recording of the momentum imaging signal and the CEP signal is achieved.

2.7 Programs for the data acquisition and analysis

2.7.1 Overview

The data acquisition from the TDC8HP board is controlled by a software "CoboldPC 2011" (RoentDek Handels GmbH.). By the software, every signal input to the TDC8HP board are recorded in a binary file. A new program for the data analysis with C++ codes using microsoft foundation class was constructed.

Fig 2.20: Digital phasemeter circuit box.

2.7.2 CoboldPC 2011

In the experiments described in section 2.8 and Chapter 3, the data acquisition using the TDC8HP board is performeded by the CoboldPC software. The timing of every signals and the information of the trigger signals are recorded in a binary file (List Mode File, "(filename).lmf"). With the CoboldPC, the histogram of the ion count rate and the position of the detection can be shown during the data accumulation. The conditions of the data acquisition and the data analysis are done by running a batch file (Cobold Command File, "(filename).ccf"). For the data acquisition, one ccf file is made to determine the conditions of the acquisition and the data analysis, and the number of the data for the acquisition and the name of the lmf file are given.

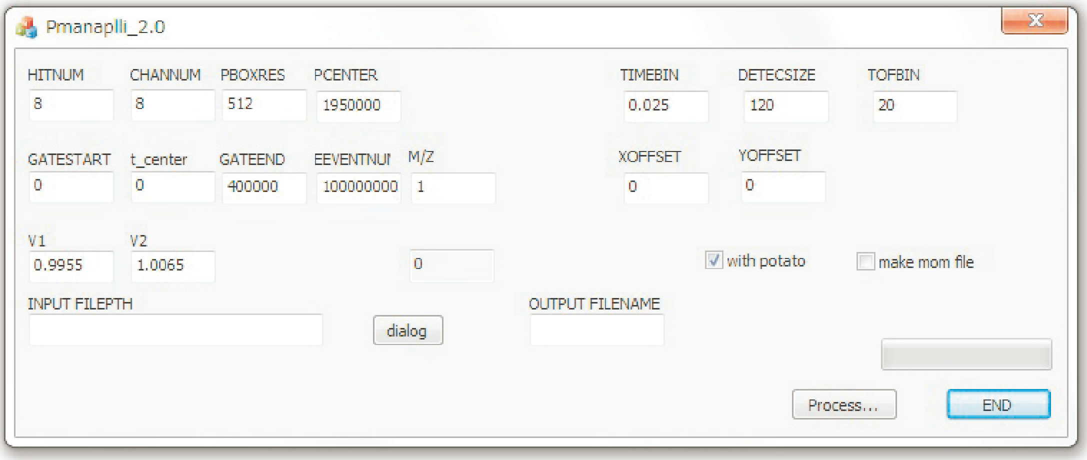

Fig 2.21: Dialog box of the analysis program.

2.7.3 Program of the data analysis

In the present study, I developed a new program for the data analysis with C++ codes using the microsoft foundation class. The program consists of four parts; (i) parameter setting for the analysis, (ii) data reading from the lmf files, (iii) calculation of the momentum release of respective ions, and (iv) writing the results of the calculation in an output file.

The dialog box of the program is shown in Fig. 2.21 and the meaning of the parameters employed in the program is listed in Table 2.1. When the “Process” button is clicked, the *.lmf file set as an input file by the “INPUT FILEPATH” text box is opened. The timing signals for each signal channel are read. The position of the signal in the v coordinate is obtained from the signals in the channels 0 and 1, when the average of the two signals is larger than the value “GATESTART” and smaller than the value “GATEEND”. The position in the w coordinate is obtained from the signals in the channels 2 and 3. Only the two wires in the HEX120 are used to the position detection. From the position of the detection and the time of flight, the three dimensional momentum release of the ion is calculated using Eqs. (2.24) and (2.25). When the check box “with POTATO” is enabled, the asymmetry of the photoelectron emission in the phasemeter is obtained from the signals in the channnels 4 and 5, and the polar angle of each plot is calculated. When the check box “make mom file” is enabled, all of the three-dimensional momentum and the phase data are written a text file with the name set as an input the text box “OUTPUT FILENAME”.

Table 2.1: Meaning of each variable in the dialog box of the program.

Variable	meaning
HITNUM	The number of the signal recorded in a channel by one laser shot
CHANNUM	The number of the channels to be analyzed
PBOXRES	The resolution of the output of the digital circuit
PCENTER	The timing of the signals in the channels 4 and 5 when the asymmetry is zero
GATESTART	The lower limit of the signal timing treated in the analysis
t_center	The center of the peak treated in the analysis
GATEEND	The upper limit of the signal timing to be treated in the analysis
EEVENTNUM	The number of the events to be analyzed
M/Z	The mass to charge ratio of the signal in the analysis
V1	The half value of the signal propagation velocity in the v-wire (mm/ns)
V2	The half value of the signal propagation velocity in the w-wire (mm/ns)
TIMEBIN	The time corresponds to one unit of the TDC board (ns)
DETECSIZE	The diameter of the detector (mm)
TOFBIN	The size of the bin in the output tof spectrum (unit)
XOFFSET	The x position of the momentum zero on the detector (mm)
YOFFSET	The y position of the momentum zero on the detector (mm)
with potato	Whether the CEP data are analyzed or not
make mom file	Whether the momentum data are saved or not
INPUT FILEPATH	The file path of the analyzed data file
OUTPUT FILENAME	The name of the output data files

2.8 Asymmetry in D_2 dissociation

2.8.1 overview

In these several years, asymmetric ion emission from molecular ions generated by few-cycle pulses have been studied intensively [9, 10]. Especially, D^+ emission from D_2 ionized and excited through the re-collision process showed salient CEP-dependent asymmetry [2]. In the present section, the CEP dependence of the D^+ ejection from D_2 is investigated in order to check the performance of our new experimental setup.

2.8.2 Experiment

A sample gas of D_2 is introduced into the momentum imaging chamber. Few-cycle laser pulses with the pulse energy of ~ 70 μJ/pulse are focused on the sample gas. The peak intensity at the focus is estimated to be $\sim 4.2 \times 10^{14}$ W/cm^2. The ion count rate is ~ 2 counts/shot and the data is accumulated for 1.9×10^7 laser shots.

2.8.3 Results

Figures 2.22 and 2.23 show the momentum images of D^+ ions emitted when D_2 is irradiated with few-cycle laser pulses accumulated for all CEP values-. On the basis of the magnitude of the momentum release, the dissociation pathway through which D^+ is produced is assigned to $D_2^+ \rightarrow$ D + D^+. In the upper and lower areas of the momentum image, D^+ with the high momentum release larger than 35×10^3 u m/s can be identified, which is assigned to the recollision excitation process to the dissociative state of D_2^+.

Figure 2.24 shows the momentum image when the relative CEP values are in the range of $0.2 \sim 0.4\pi$. As can be seen clearly, the D^+ emission yield I_{A} in the area A is significantly larger than the yield I_{B} in the area B. Contrary, the momentum image of the

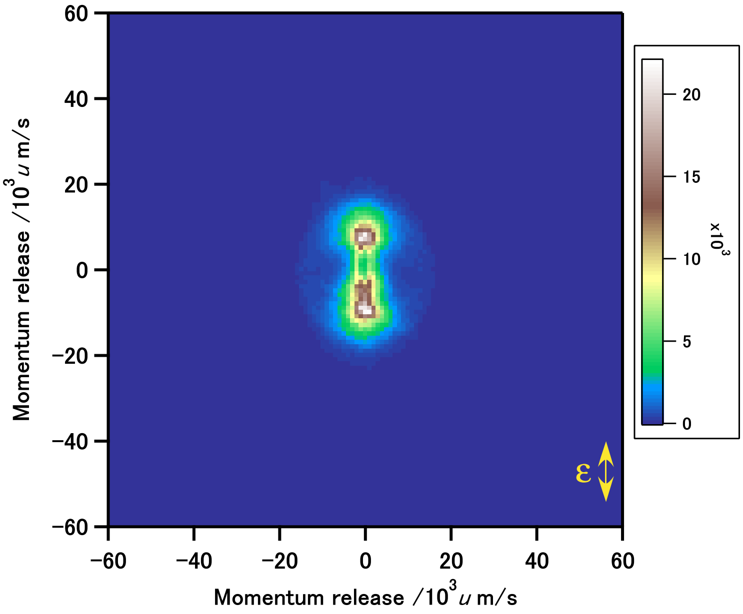

Fig 2.22: Momentum image of D^+ emitted from D_2 accumulated for all CEP values.

D^+ emission obtained when the relative CEP values are in the range of $1.2 \sim 1.4\pi$ shown in Fig. 2.25 exhibits an opposite tendency, that is, the yield I_B in the area B is larger than the yield I_A in the area A.

In order to estimate the asymmetry of the D^+ emission, the asymmetry parameter P_{asym} is defined as

$$P_{\mathrm{asym}} = \frac{I_A - I_B}{I_A + I_B}, \tag{2.26}$$

and P_{asym} values are plotted in Fig. 2.26 as a function of the relative CEP value. As shown in this figure, a clear CEP dependence can be seen in the D^+ emission from D_2. The degree of the asymmetry ~ 0.15 is slightly smaller than the value reported in the previous study ~0.2 [2]. The reason of the smaller asymmetry may be ascribed to a volume averaging effect as well as to the difference in the temporal shape of the few-cycle laser pulses.

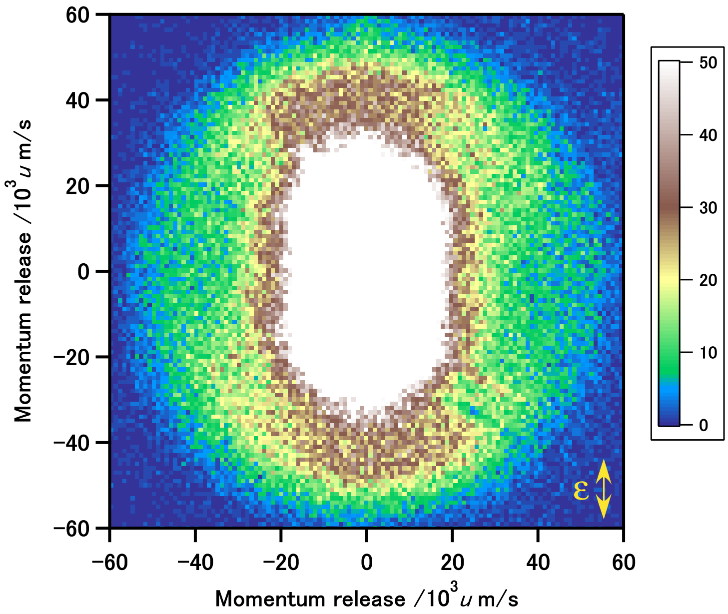

Fig 2.23: Same as Fig. 2.22 but with different color scale.

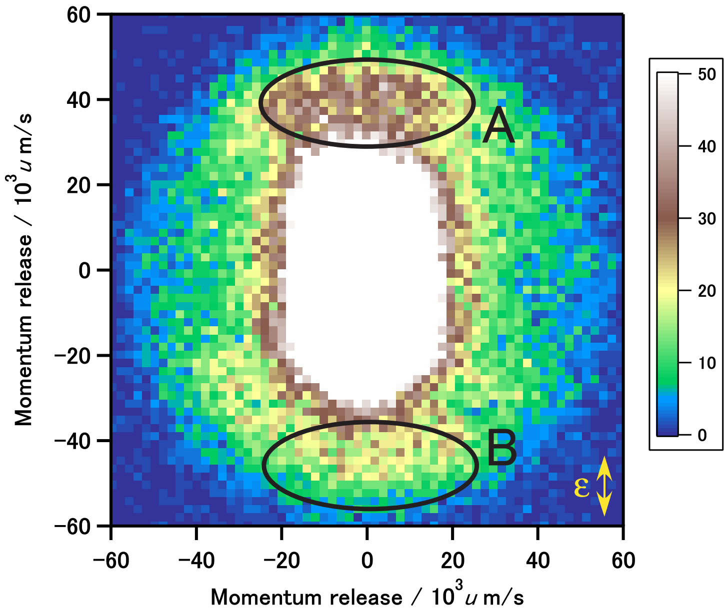

Fig 2.24: Momentum image of D^+ emitted from D_2 at the relative CEP that gives the maximum extent of asymmetry.

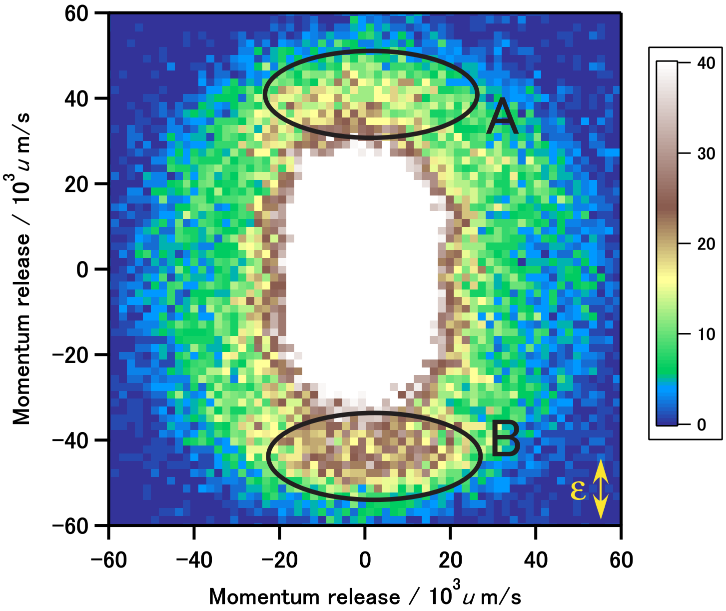

Fig 2.25: Momentum image of D^+ emitted from D_2 when the relative CEP is shifted by π different from that in Fig. 2.24.

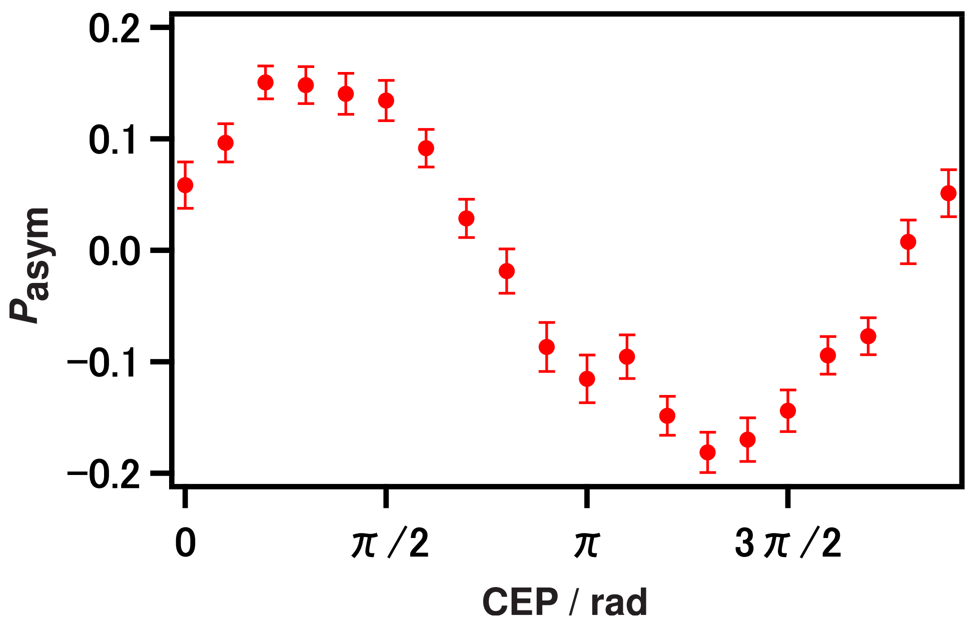

Fig 2.26: CEP dependence of the asymmetry in the D^+ emission from D_2.

References

[1] G. G. Paulus, F. Lindner, H.Walther, A. Baltuska, E. Goulielmakis, M. Lezius and F. Krausz, *Phys. Rev. Lett.*, **91**, 253004 (2003).

[2] M. F. Kling, Ch. Siedschlag, A. J. Verhoef, J. I. Khan, M. Schultze, Th. Uphues, Y. Ni, M. Uiberacker, M. Drescher, F. Krausz and M. J. J. Vrakking, *Science*, **312**, 246 (2006).

[3] T. Wittmann, B. Horvath, W. Helml, M. G. Schatzel, X. Gu, A. L. Cavalieri, G. G. Paulus and R. Kienberger, *Nat. Phys.*, **5**, 357 (2009).

[4] G. Cheriaux, P. Rousseau, F. Salin, J. P. Chambaret, B. Walker and L. F. Dimauro *Opt. Lett.*, **21**, 414 (1996).

[5] W. H. Knox, R. L. Fork, M. C. Downer, R. H. Stolen, C. V. Shank and J. A. Valdmanis *Appl. Phys. B*, **46**, 12 (1985).

[6] M. Nisoli, S. Stagira, S. De Silvestri, O. Svelto, S. Sartania, Z. Cheng, M. Lenzner, Ch. Spielmann and F. Krausz, *Appl. Phys. B*, **65**, 189 (1997).

[7] W. C. Wiley and I. H. Mclaren *Rev. Sci. Intsl.*, **26**, 1150 (1955).

[8] A. T. J. B. Eppink and D. H. Parker, *Rev. Sci. Instrum.*, **68**, 3477 (1997).

[9] I. Znakovskaya, P. von den Hoff, S. Zherebtsov, A. Wirth, O. Herrwerth, M. J. J. Vrakking, R. de Vivie-Riedle and M. F. Kling *Phys. Rev. Lett.*, **103**, 103002 (2009).

[10] Y. Liu, X. Liu, Y. Deng, C. Wu, H. Jiang and Q. Gong, *Phys. Rev. Lett.*, **106**, 073004 (2011).

Chapter 3. CEP dependent asymmetric dissociation of C_2D_2

インターネット公表に関する共著者全員、および、雑誌社からの承認が得られていないため、本章については、非公開。

"Carrier-envelope-phase dependence of asymmetric C-D bond breaking in C_2D_2 in an intense few-cycle laser field"

Chemical Physics Letters, 595,596 号　61-66 頁

Chapter 4. Conclusions and future perspective

When molecules are irradiated with the intense laser pulses, not only ionization and dissociation but also chemical bond rearrangement can be induced. One of the most interesting processes is ultrafast hydrogen migration within a hydrocarbon molecule. It has been shown that the hydrogen migration proceeds on the time scale of several tens of femtosecond or shorter [1-5], but this ultrafast chemical bond rearrangement process has not sufficiently been explored. An idea to treat hydrogen atoms as wave functions was proposed [6] and was demonstrated by numerical calculations [7]. Because the mass of a hydrogen atom is small its motion within a molecule can be sensitively influenced by the change in the charge distribution induced by a few-cycle pulse, and therefore, the hydrogen migration may exhibit a CEP dependence. Investigation of the CEP dependence of hydrogen migration processes may give us further information on the very early stage of molecules interacting with an intense laser field.

From pump-probe measurements using few-cycle pulses, we can investigate ultrafast dynamics of molecules. For example, the dissociation processes of diatomic molecules such as N_2 and O_2 [10] and the isomerization of acetylene [11] were investigated by such a pump-probe method. If CEP characterized few-cycle pules are adopted for pump-probe measurements, we will be able to learn more precisely how electrons and nuclei interact in the laser field on the basis of CEP dependences.

In the simulation in Chapter 3 of this thesis, several approximations were adapted. One of the important approximations is the strong field approximation (SFA), in which the Coulomb attraction between the ejecting electron and the remaining ion core is neglected. However, as has been reported [8, 9], the Coulomb attraction needs to be taken into account. In the case of molecules, the Coulomb correction is more difficult to be implemented than in the case of atoms because of the anisotropic Coulombic field within a molecule. Because the Coulomb attraction is expected to be changed in response to the variation of the electric field of light, measurements of CEP dependent phenomena may give us valuable information on the Coulomb attraction effect within a molecule.

References

[1] A. Hishikawa, H. Hasegawa and K. Yamanouchi *J. Elect. Spec. Relat. Phenom.*, **141**, 195-200 (2004).

[2] R. Itakura, P. Liu, Y. Furukawa, T. Okino, K.. Yamanouchi, and H. Nakano *J. Chem. Phys.*, **127**, 104306 (2007).

[3] H. Xu, C. Marceau, K. Nakai, T. Okino, S.L. Chin and K. Yamanouchi *J. Chem. Phys.*, **133**, 071103 (2010).

[4] R. Kanya, T. Kudou, N. Schirmel, S. Miura, K.-M. Weitzel, K. Hoshina and K. Yamanouchi *J. Chem. Phys.*, **136**, 204309 (2012).

[5] T. Okino, A. Watanabe, H. Xu and K. Yamanouchi *Phys. Chem. Chem. Phys.*, **14**, 10640 (2012).

[6] T. Kato and K. Yamanouchi, *J. Chem. Phys.*, **131**, 164118 (2009).

[7] T. Kato and K. Yamanouchi, Phys. Rev. A, **85**, 034504 (2012).

[8] S. Chelkowski and A. D. Bandrauk, *Phys. Rev. A*, **71**, 053815 (2005).

[9] X. Xie, S. Roither, S. Gräfe, D. Kartashov, E. Persson, C. Lemell, L. Zhang, M. S. Schöffler, A. Baltuska, J. Burgdörfer and M. Kitzler, *N. Jour. Phys.*, **15**, 043050 (2013).

[10] I. A. Bocharova, A. S. Alnaser, U. Thumm, T. Niederhausen, D. Ray, C. L. Cocke and I. V. Litvinyuk *Phis. Rev. A*, **83**, 013417 (2011).

[11] A. Matsuda, M. Fushitani, E. J. Takahashi and A. Hishikawa, *Phys. Chem. Chem. Phys.*, **13**, 8697 (2013).

[12] A. J. Verhoef, A. V. Mitrofanov, X. T. Nguyen, M. Krikunova, S. Fritzsche, N. M. Kabachnik, M. Drescher and A. Baltuska, *N. Jour. Phys.*, **13**, 113003 (2011).

[13] W. Cao, S. De, K. P. Singh, S. Chen, M. S. Schöffler, A. S. Alnaser, I. A. Bocharova, G. Laurent, D. Ray, S. Zherebtsov, M. F. Kling, I. Ben-Itzhak, I. V. Litvinyuk, A. Belkacem, T. Osipov, T. Rescigno and C. L. Cocke *Phys. Rev. A*, **82**, 043410 (2010).

[14] X. Zhou, P. Ranitovic, C.W. Hogle, J. H. D. Eland, H. C. Kapteyn and M. M. Murnane, *Nat. Phys.*, **8**, 232 (2012).

[15] D. M. Tapia, M. Vacher, M. J. Bearpark and M. A. Robb, *J. Chem. Phys.*, **139**, 044110 (2013).

Acknowledgments

First of all, I would like to thank Prof. Kaoru Yamanouchi for his supervision. He gave me a lot of valuable advice, and encouraged me throughout the thesis study. I am truly grateful to him for having given me an ideal research environment. I am also indebted to Dr. Tomoya Okino and Dr. Atsushi Iwasaki for their valuable guidance in the experiments. I am also grateful to other staff members in Prof. Yamanouchi's group, Prof. Tsuyoshi Kato, Prof. Huailiang Xu, Dr. Reika Kanya, Dr. Takahiro Sato, and Dr. Akinori Sugiyama.

I would like to thank Prof. Gerhard G. Paulus, Mr. Tim Rathje, and Mr. Dominik Hoff in Friedrich-Schiller-Universität, Jena for their kind cooperation in the CEP-tagging experiments, Prof. Mauro Nisoli and Prof. Giuseppe Sansone in Politecnico di Milano for their guidance in the generation of few-cycle pulses, and Prof. Andrius Baltuska and Dr. Markus Kitler in Vienna University of Technology for their helpful cooperation in the joint experiments.

More gratitude also goes out to our experimental team, Mr. Toshiaki Ando, Mr. Kazuki Ootaka, Mr. Masato Obuchi, Mr. Akihiro Shimamoto and Ms. MIkoto Toyama, and to all the members of Prof. Yamanouchi's group. Last but not least, I am grateful to my family members and to my friends for their warm support.